Electronic Supplementary Information

ALD/MLD coating of patterned vertically aligned carbon nanotube micropillars with Fe-NH₂TP hybrids

[a]R. M. Silva*, [b]J. Rocha*, [a]R. F. Silva

[a]CICECO - Aveiro Institute of Materials, Department of Materials and Ceramic Engineering, University of Aveiro, 3810-193 Aveiro, Portugal

[b]CICECO - Aveiro Institute of Materials, Department of Chemistry, University of Aveiro, 3810-193 Aveiro, Portugal

Materials

Single-side polished silicon (Si(100)) wafers from SILTRONIX with 300 nm of thermally grown SiO_2 (Si/SiO₂) were used as substrates. Ni target (Goodfellow, 99% purity). Argon (Ar, Air Liquide, 99% purity), hydrogen (H_2, Air Liquide, 99.9% purity), acetylene (C_2H_2, Air Liquide, 99% purity) and nitrogen (N_2, Air Liquide, 99% purity). Fe(III)-tris(2,2,6,6-tetramethyl-3,5-heptanedionate) complex, (Fe(thd)₃, STREM Chemicals, 99%) and 2-aminoterephthalic acid, (NH₂TPA, Sigma Aldrich, 99% purity). Titanium (IV) tetraisopropoxide (TTIP, STREM Chemicals, 98% purity) and de-ionized water (Milli-Q). All chemicals were used as received.

Characterization

The NH₂-MIL101 (Fe) powdered sample diffraction pattern was collected on a powder X-ray diffractometer (PANalytical Empyrean) using Cu-Kα1 radiation (0.1540 nm, 45 kV, 40 mA) in the transmission spinning scan mode in the range 0° - 20° (2θ) with a 0.02° step.

Thermal chemical vapor deposition (T-CVD) processing

The carbon nanotubes growth process by T-CVD involves heating a catalytic metal at elevated temperatures in a tube furnace, using a carbon gas source through the tube reactor, over a period of time. In this manner, the continuous Ni thin film is broken into catalytically active nano-sized particles (*e.g.*, by annealing under a reductive atmosphere; step 2) from where the nanotubes nucleation takes place. The general mechanism in this process is the dissociation of the carbon gas source molecules, catalyzed by the Ni, and saturation of carbon atoms in the Ni nano-sized particles. Precipitation of carbon from the former particles leads to the formation of CNTs (step 3), as schematically shown in Figure S1. The step 1 and 4 indicates heating and cooled down stage, respectively.
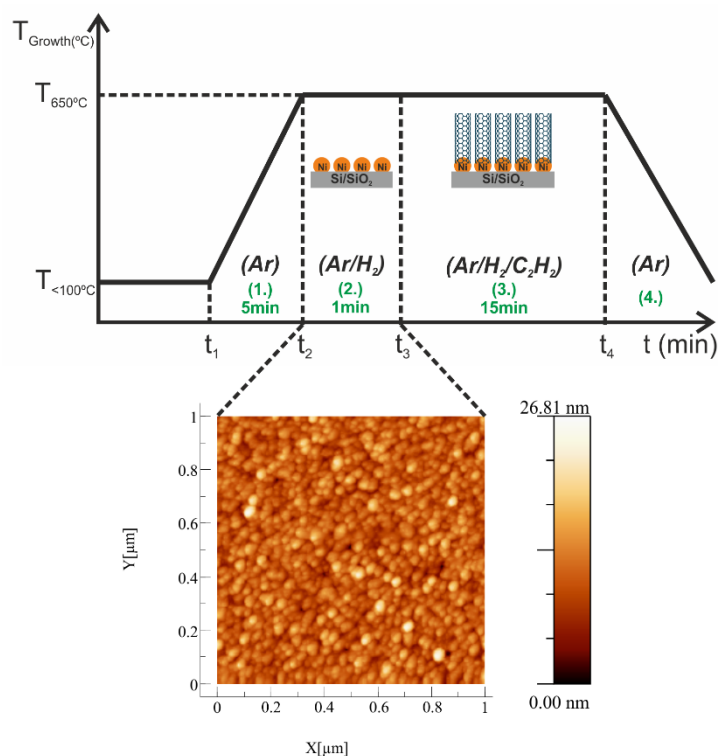
Figure S1. Schematic representation of the carbon nanotubes growth process, involving different steps over a period of time. The AFM image (1 μm x 1 μm) reveals the Ni catalyst nano-sized particles prior to the nanotubes growth and they appear as granular film, presenting a root-mean-square (Rq) roughness of 2.95 nm. It is worth to note that to minimize the morphology alteration during the cooling process, the catalyst was quenched rapidly to room temperature, after the step 2. Subsequently, the sample was taken out of the chamber and characterized by an AFM

**Table S1.** ALD/MLD or ALD processes based on Fe precursors.

Iron (Fe)	Organic	Deposition temperature T(ºC)	Year	Ref.
FeCl$_3$, Fe(acac)$_3$	TPA	240 – 260 ºC	2018	[1]
FeCl$_3$	TPA	250 – 360 ºC	2020	[2]
FeCl$_3$	TPA	280 ºC	2020	[3]
Fe(thd)$_3$	2-NH$_2$TP	170 – 250 ºC	This work	
Iron (Fe)	Oxygen source	Deposition temperature T(ºC)	Year	Ref.
Fe(thd)$_3$	O$_3$	160 – 330 ºC	2005	[4]
Fe(thd)$_3$	O$_3$	250 ºC	2020	[5]

TPA – terephthalic acid or BDC – 1,4-benzenedicarboxylic acid.

Fe-NH$_2$TP on Si/SiO$_2$ support
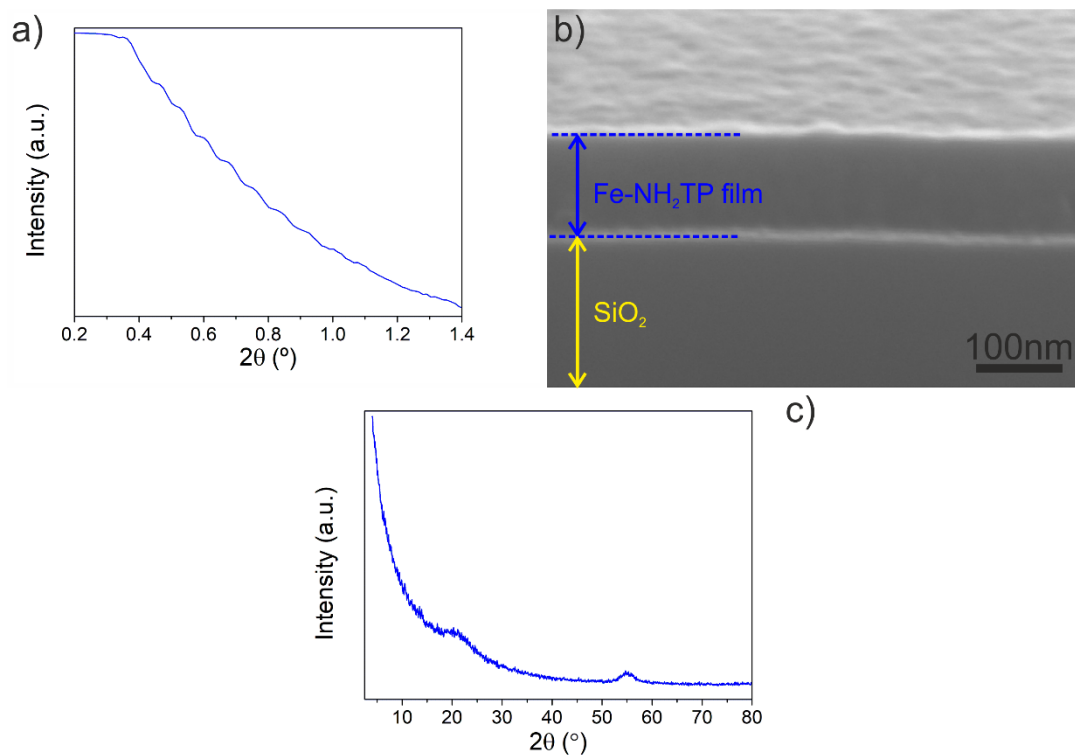
Figure S2. (a) XRR pattern of Fe-NH$_2$TP thin film after 1000 ALD/MLD cycles at 180 ºC, and (b) cross-section SEM image of this film. The film thickness is ca. 126 nm. The SEM image is tilted 7º and the thickness measurement took this into consideration. (c) GIXRD pattern of the same film; the observed broad reflections are assigned to the Si(100) substrate with 300 nm of thermally grown SiO$_2$, *i.e.*, the features at 20-25º and 50-60º are assigned to the SiO$_2$ layer and the characteristic (311) plane of the crystalline Si(100), respectively.
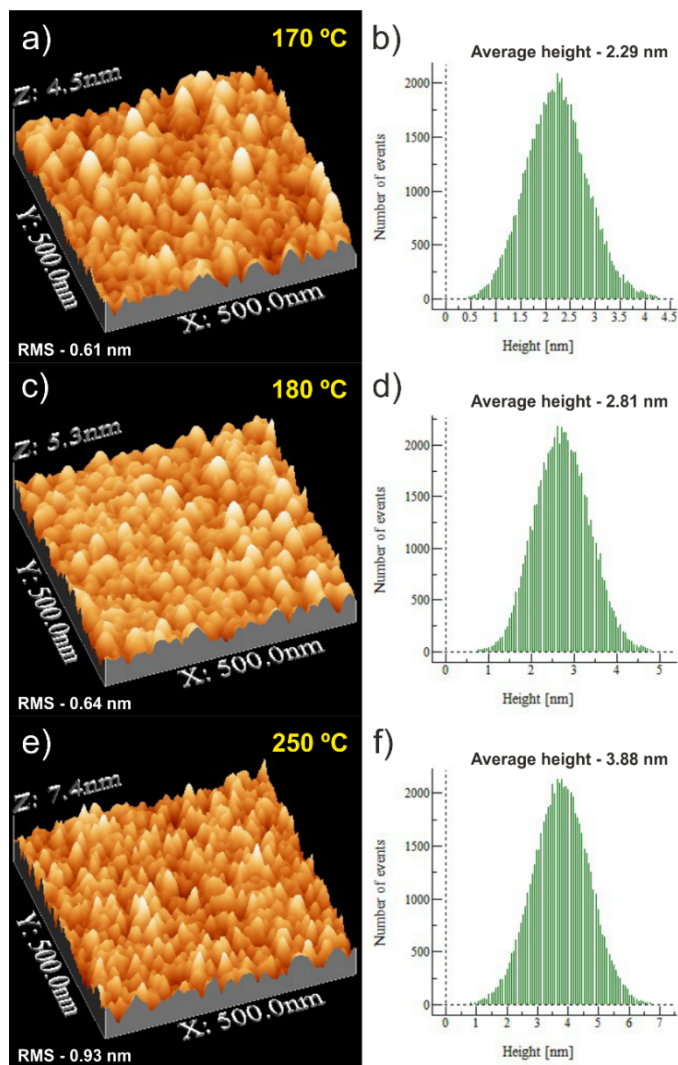
Figure S3. 3D rendered AFM images of the Fe-NH$_2$TP thin films after 1000 ALD/MLD cycles at the temperatures depicted and the corresponding histograms of height distribution of surface roughness. The deposition temperature induces smaller *Rq* values and the height distribution is symmetric, witnessing the homogenous distribution of the hills and valleys in deposited thin films.

The NH$_2$-MIL101 (Fe) powdered sample was synthesized according to the experimental procedure reported in Ref. [6].
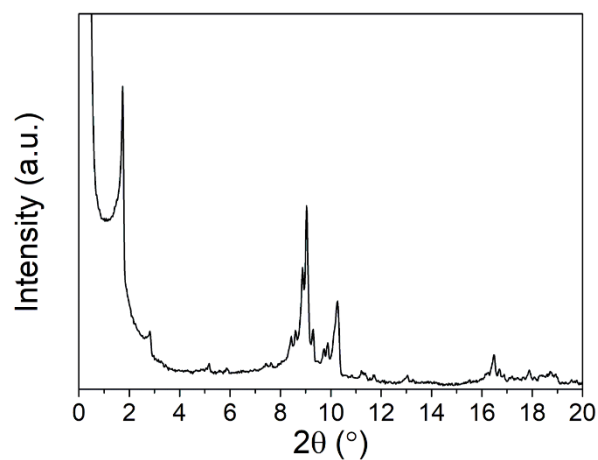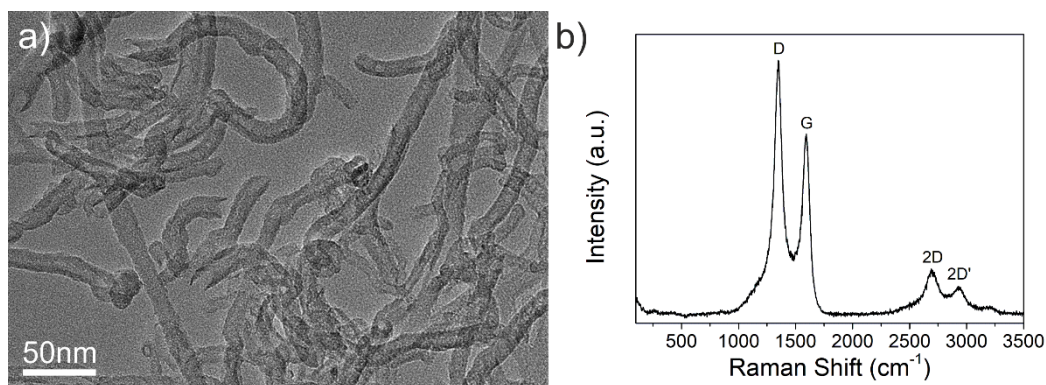

Figure S4. Experimental powder XRD pattern of NH$_2$-MIL101 (Fe) powdered sample showing the characteristic reflection at ca. 1.7° that confirms the formation of the NH$_2$-MIL101 (Fe) structure, in agreement with the literature [6,7].
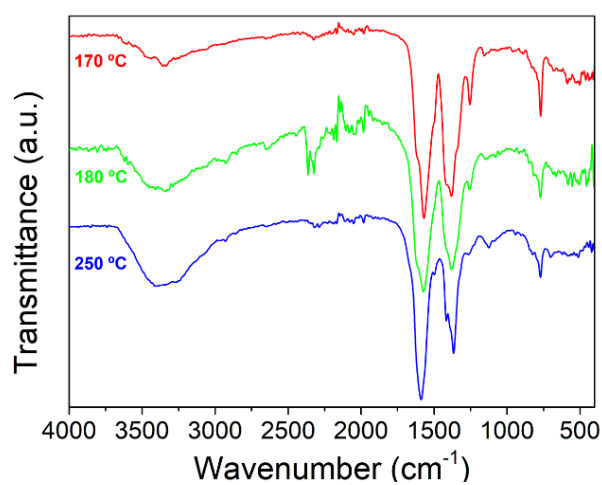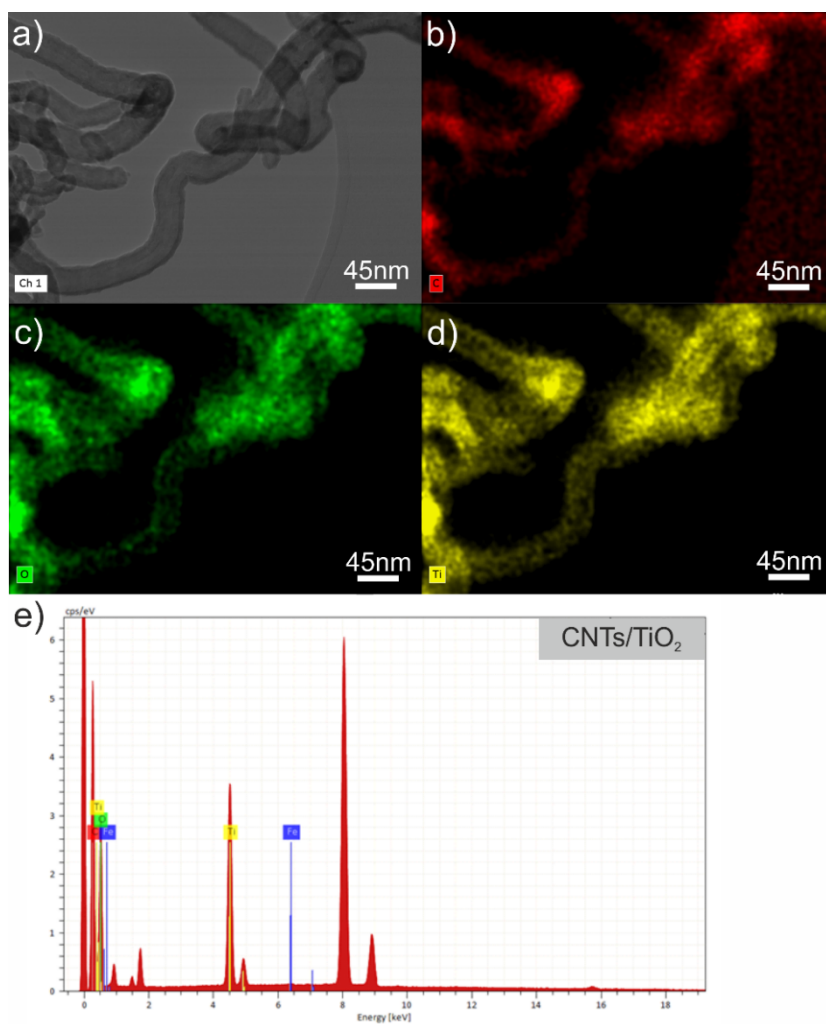

Figure S5. Normalized ATR-FTIR spectra at the deposition temperatures depicted, after 1000 ALD/MLD cycles.

Fe-NH₂TP on TiO₂/VA-CNTs

Figure S6. (a) BF-TEM image and (b) Raman spectrum of the uncoated nanotubes. The TEM image confirms that the as-prepared nanotubes are multiwalled corroborating with the Raman characteristic D-band and G-band peaks [8,9].


Figure S7. (a) TE-STEM mode image and EDX elemental mapping of (b) C, (c) O and (d) Ti. (e) EDX spectrum of the carbon nanotubes coated with TiO_2, after 200 ALD cycles at 100 ºC.
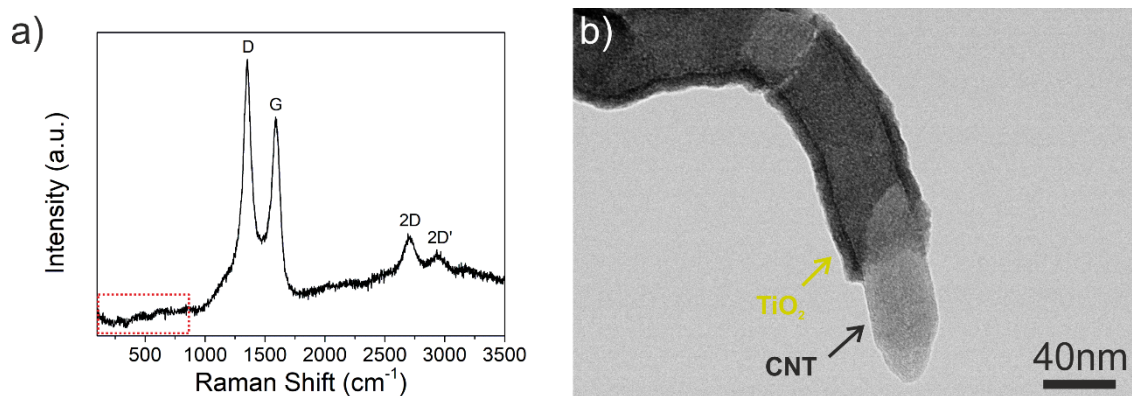
Figure S8. (a) Raman spectrum of carbon nanotubes coated with amorphous TiO_2 after undergoing 200 ALD cycles at 100 °C. The dashed square highlights the region where crystalline TiO_2 modes, such as the anatase phase, were anticipated [10]. The detected modes are attributed to the nanotubes, exhibiting no significant alterations to their shape. (b) STEM showcases an individual coated nanotube (TiO_2 shell formation).
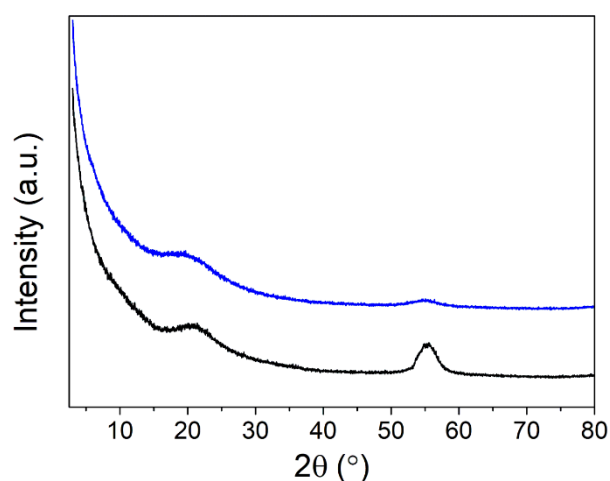
Figure S9. Experimental GIXRD pattern of the thin films: TiO_2 after 200 ALD cycles at 100 °C (black line, TiO_2/ Si/SiO_2) and $Fe-NH_2TP$ after 1000 ALD/MLD cycles at 180 °C (blue line, $Fe-NH_2TP/TiO_2/Si/SiO_2$). The broad reflections are assigned to the Si/SiO_2 of the substrate.
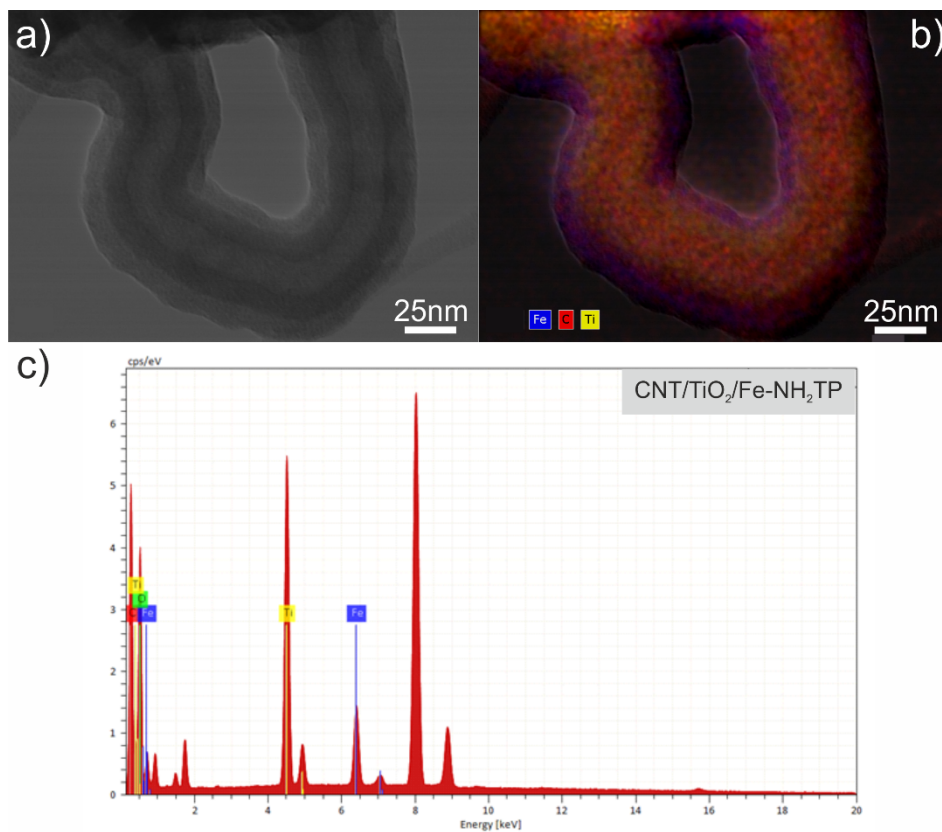
Figure S10. (a) TE-STEM mode image, (b) EDX Fe, C and Ti mapping, and (c) EDX spectrum of CNT/TiO$_2$/Fe-NH$_2$TP composites, highlighting the continuous surface coverage of the nanotubes with Fe-NH$_2$TP thin film.
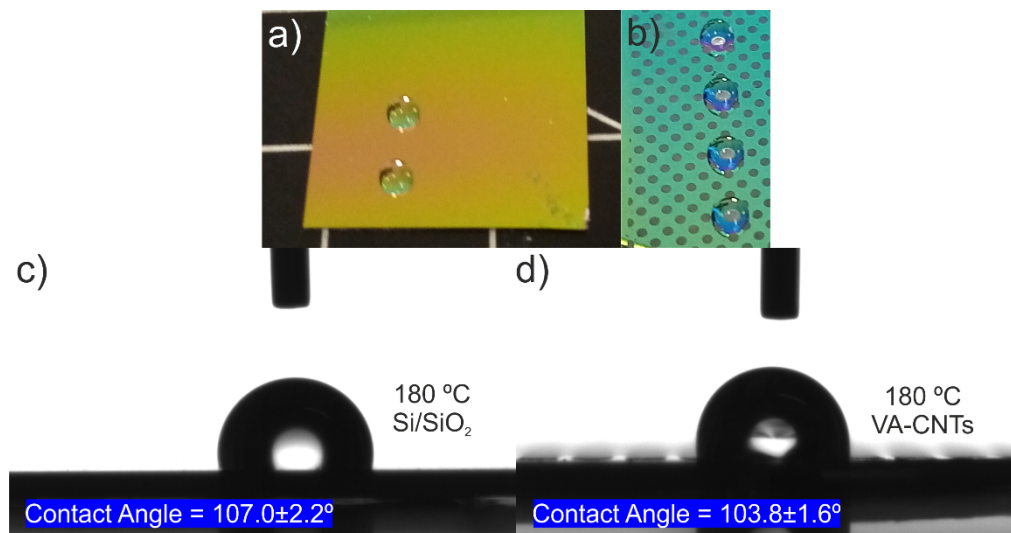
Figure S11. (a) Photographs of 3 µL water droplets on hydrophobic Fe-NH$_2$TP (180 ºC) thin film over (a,c) Si/SiO$_2$ support, and over (b,d) carbon nanotube micropillars.

Thin film density

The Fe-NH$_2$TP thin film density (ρ_m) can be estimated from the X-ray reflectance critical angle (θ_c) as follows [11]:

$$\rho_e = \frac{\theta_c^2 \pi}{\lambda^2 r_e} (e^- \, m^{-3})$$

(1)

where λ is the X-ray wavelength and r_e is the classical electron radius.

$$\rho_m = \frac{\rho_e A}{N_A Z} (g \, m^{-3})$$

(2)

where A is the average of molecular weight, Z is the average of atomic number and N_A is the Avogadro constant. The density (ρ_m) value was estimated to be 1.58 g cm^{-3}.

References for ESI

[1] A. Tanskanen, M. Karppinen, *Sci. Rep.*, 2018, **8**, 8976.

[2] A. Khayyami, A. Philip, J. Multia, M. Karppinen, *Dalton Trans.*, 2020, **49**, 11310-11316.

[3] A.Philip, J-P. Niemelä, G. C. Tewari, B. Putz, T. E. J. Edwards, M. Itoh, I. Utke, M. Karppinen, ACS *Appl. Mater. Interfaces.*, 2020, **12**, 21912-21921.

[4] M. Lie, H. Fjellvåg, A. Kjekshus, *Thin Solid Films*, 2005, **488**, 74-81.

[5] A. Brennhagen, K. B. Kvamme, K. S. S. Sverdlilje, O. Nilsen, *Solid State Ion.*, 2020, **353**, 115377.

[6] X. Y. Dao, J.H. Guo, Y-P. Wei, F. Guo, Y. Liu, W-Y. Sun, *Inorg. Chem.*, 2019, **58**, 8517-8524.

[7] S. Bauer, C. Serre, T. Devic, P. Horcajada, J. Marrot, G. Férey, N. Stock, *Inorg. Chem.*, 2008, **47**, 7568-7576.

[8] A. C. Ferrari, J. Robertson, Phys. Rev. B, 2000, **20**, 14095.

[9] M. S. Dresselhaus, G. Dresselhaus, R. Saito, A. Jorio, Phys. Rep., 2005, **409**, 47-99.

[10] I. E. Oliveira, R. M. Silva, J. Rodrigues, M. R. Correia, T. Monteiro, J. Faria, R. F. Silva, C. G. Silva, *RSC Advances*, 2022, **12**, 16419-16430.

[11] J. Penttinen, M. Nisula, M. Karppinen, *Chem. Eur. J.*, 2019, **25**, 11466-11473.